## Glaucoma

# Angular Location of Retinal Nerve Fiber Layer Defect: Association With Myopia and Open-Angle Glaucoma

Eunoo Bak,[1,2] Kyoung Min Lee,[1,3] Martha Kim,[4] Sohee Oh,[5] and Seok Hwan Kim[1,3]

[1]Department of Ophthalmology, Seoul National University College of Medicine, Seoul, Korea
[2]Department of Ophthalmology, Seoul National University Hospital, Seoul, Korea
[3]Department of Ophthalmology, Seoul National University Boramae Medical Center, Seoul, Korea
[4]Department of Ophthalmology, Dongguk University Ilsan Hospital, Goyang, Korea
[5]Department of Biostatistics, Seoul National University Boramae Medical Center, Seoul, Korea

PURPOSE. To compare retinal nerve fiber layer (RNFL) defects' angle measurements determined from the center of the optic disc and Bruch's membrane opening (BMO), as a function of myopia and open-angle glaucoma (OAG) subtypes.

METHODS. In total, 118 patients with OAG were grouped by axial length (AL; high myopia, AL >26 mm; mild to moderate myopia, 24 ≤ AL ≤26 mm; nonmyopia, AL <24 mm) and OAG subtype (normal-tension glaucoma [NTG], high-tension glaucoma [HTG]). The disc and BMO centers were determined by a merged image of red-free fundus photography and spectral-domain optical coherence tomography. The angular location of the RNFL defect close to the fovea (angle $\alpha$) was measured from the disc center and BMO center, respectively (angle $\alpha_{disc}$ and angle $\alpha_{BMO}$). The difference between angle $\alpha_{disc}$ and $\alpha_{BMO}$ ($\Delta\alpha$), as well as the RNFL defect width (angle $\gamma$), was evaluated.

RESULTS. Angle $\alpha_{disc}$ was smaller in myopic eyes and correlated significantly with AL ($P = 0.001$), whereas it did not differ among OAG subgroups. Angle $\alpha_{BMO}$ and angle $\gamma$ were not different in the myopic and OAG subgroups. The $\Delta\alpha$ was larger for eyes with higher degree of myopia and had significant correlation with AL ($P < 0.001$) and was larger in NTG eyes than in HTG eyes ($P = 0.023$).

CONCLUSIONS. The angular location of the RNFL defect measured from the disc center, but not from the BMO center, was closer to the fovea for glaucomatous eyes with higher values of AL. The present study may facilitate understanding of the characteristic locational pattern of the RNFL defect in myopic glaucomatous eyes.

Keywords: glaucoma, retinal nerve fiber layer defect, myopia, optic disc, Bruch's membrane opening

Glaucoma is a progressive optic neuropathy characterized by degeneration of the retinal ganglion cells (RGCs).[1] The lamina cribrosa (LC) plays a critical role as the main site of RGC damage in glaucoma pathogenesis.[2,3] RGC-axonal injury clinically leads to structural changes of the optic disc, retinal nerve fiber layer (RNFL) defects, and functional loss of vision.[1,4]

The angular location of RNFL defects in glaucoma is reported to have a spatial preponderance,[2,5,6] while the exact location might be determined by several factors. Highly myopic eyes with open-angle glaucoma (OAG) are reported to have defects closer to the fovea[7–10] relative to nonmyopic eyes. However, the mechanism linking the locational pattern of the RNFL defect and myopia is not clear. In addition, there are inconsistencies in the study of OAG subtypes. Some reports have shown that localized RNFL defects in normal-tension glaucoma (NTG) were closer to the fovea than those in high-tension glaucoma (HTG),[11,12] while other studies have reported no difference in the spatial location of RNFL defects between NTG and HTG.[13–16] Therefore, the issue of which factor and

mechanism determine the spatial location of the RNFL defect in OAG remains controversial. Although our current understanding of OAG is that the arbitrary division of NTG and HTG is an oversimplification, it nonetheless continues to be used to classify them for purposes of research.

The concept of assessing optic nerve head (ONH) structure based on the Bruch's membrane opening (BMO) is recently emerging.[17] Sawada et al.[18] studied optic disc margin anatomic features in myopic eyes and reported significant misalignment between the disc and the BMO center. Also recently, in the Boramae Myopia Cohort Study, we observed longitudinal ONH change and LC shift during axial elongation along with a relatively stable posterior polar retinal structure and BMO in young myopic children, resulting in the misalignment between the disc and the BMO center.[19–21] These changes have shown strong correlation with the preferential site of the RNFL defect in NTG with myopia.[22] Therefore, we hypothesized that the angular location of the RNFL defect in myopic OAG eyes may vary between disc and BMO centers.

In this study, we comparatively investigated the angular location of the RNFL defect relative to the disc and BMO centers, respectively, in association with the degree of myopia and OAG subtypes.

## METHODS

This cross-sectional study was based on patients with OAG included in the Boramae Glaucoma Imaging Study, an ongoing prospective study at Seoul National University Boramae Medical Center (Seoul, Korea). Written informed consent to participate was obtained from all patients. The study protocol was approved by the Seoul National University Boramae Medical Center Institutional Review Board and conformed to the tenets of the Declaration of Helsinki.

### Study Participants

All of the participants underwent a full ophthalmologic examination with best-corrected visual acuity (BCVA) assessment, refraction, slit-lamp biomicroscopy, Goldmann applanation tonometry, gonioscopy, dilated funduscopic examination, keratometry (RKT-7700; Nidek, Hiroshi, Japan), axial length (AL) measurement (IOL Master version 5; Carl Zeiss Meditec, Dublin, CA), disc photography and red-free fundus photography (TRC-NW8; Topcon, Tokyo, Japan), spectral-domain optical coherence tomography (SD-OCT; Spectralis OCT, Heidelberg Engineering, Heidelberg, Germany), and standard automated perimetry (SAP; Humphrey Field Analyzer II 750, 24-2 Swedish Interactive Threshold Algorithm; Carl Zeiss Meditec).

The inclusion criteria were OAG with localized the RNFL defect. OAG diagnosis was defined as follows: the presence of glaucomatous optic disc damage (e.g., focal notching, thinning of rim, and the RNFL defect), a glaucomatous visual field (VF) defect corresponding to structural damage, and an open angle. Localized RNFL defect was defined as a well-outlined, dark, wedge-shaped, and not spindle-like defect touching the optic disc border.[23] Glaucomatous VF defect was defined as (1) outside-normal-limits glaucoma hemifield test results or (2) three abnormal points, with a *P* value <5% probability of being normal and one with a *P* value <1% by pattern deviation or (3) pattern standard deviation of <5%. Visual field defects were confirmed on two consecutive reliable tests (fixation loss rate of ≤20%, false-positive and false-negative error rates of ≤25%).

The exclusion criteria were BCVA of <20/40, secondary OAG (i.e., steroid induced glaucoma), pathologic myopic changes that can deform the contour of the eyeball (e.g. posterior staphyloma), a history of ocular surgery other than cataract extraction or corneal refractive surgery, retinal or neurologic disease that could cause visual field defect, and a poor-quality image (i.e., quality score <15) of any section on enhanced depth imaging (EDI) SD-OCT radial scans, when the RNFL defect margin could not be delineated on red-free fundus photography and/or mean deviation (MD) <−14 dB in SAP to exclude advanced disease. If both eyes were eligible, one eye was randomly selected as the study eye.

Patients with OAG were categorized into NTG and HTG according to the IOP values. Prior to the treatment, diurnal IOP was measured repeatedly (typically five times) on the same day or on different days. The average value, which was defined as the baseline IOP, was used for the subsequent analysis. Patients with IOP ≤21 mm Hg at any point before

or after treatment were defined as NTG patients, while the others were defined as HTG patients. Further, all of the patients were divided into three groups according to the degree of myopia as classified by AL measurement[24,25]: (1) high myopia with AL longer than 26 mm, (2) mild to moderate myopia with AL between 24 and 26 mm, and (3) nonmyopia with AL shorter than 24 mm. We compared the RNFL defect among subgroups by AL or between OAG subtypes.

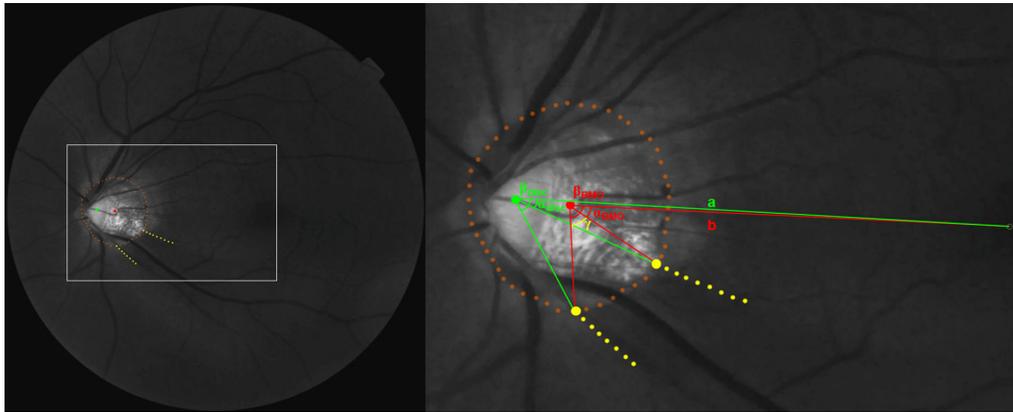### Assessment of Red-Free Fundus Photographs

Throughout the study, the assessment of RNFL was performed independently by two glaucoma specialists (EB, KML) experienced in the RNFL defect evaluation. Red-free fundus photographs were acquired using a digital fundus camera system (TRC-NW8; Topcon, Tokyo, Japan) with a green filter inserted to enhance the RNFL. The photographs were obtained after dilation of the pupil. In each red-free fundus photograph, the start point and end point of the RNFL defect were traced manually. In cases of disagreement resulting from very subtle difference on photography, the final decision was made by a third observer (SHK) consulted to achieve consensus.

### Assessment of Optic Disc Center

Measurements were made from the disc margins of red-free fundus photography, defined as the inner border of the peripapillary scleral ring. The original image was applied to the ImageJ software (V.1.48; developed by Wayne Rasband, National Institutes of Health, Bethesda, MD). The clinically visible optic disc margin was segmented independently by two glaucoma specialists (EB and KML). Images were evaluated in a masked fashion, without knowledge of the patients' clinical diagnosis or of any other clinical information. Once the margin was obtained, the optic disc center was determined by using the "centroid function" of ImageJ software. This function averages the x and y coordinates of all of the pixels in the selected margin and provides the x and y coordinates of the center in pixels.[26,27] The mean value of the two measurements was determined as the optic disc center and used for analysis. The distance between the optic disc center and BMO center was also measured in pixels using ImageJ software.

### Assessment of SD-OCT

The deep ONH complex was evaluated by SD-OCT after pupil dilation. During the acquisition of SD-OCT images, patients were asked to fixate on the target, and images were acquired with extra care for the forehead and chin stabilized by the headrest without movement. The corneal curvature of each eye was entered into the SD-OCT system before performing SD-OCT scanning so as to compensate for potential magnification error. The Glaucoma Module Premium Edition of the Spectralis machine enables detection of the BMO. Based on 24 high-resolution radial scan images of the ONH 15° apart from each other, each averaged from 24 individual B-scans, SD-OCT automatically detected the margin of the BMO. For each SD-OCT scan, one glaucoma specialist (EB) checked the automated segmentation of BMO margin, and it was corrected manually when necessary. Based on the BMO margin, the internal software determined the center of the BMO. The fovea was identified automatically aligned with a foveal-BMO axis as a reference.

**Figure 1.** Angular parameters of the RNFL photography. (*Left*) Red-free fundus photograph and infrared fundus image with delineated BMO margin merged. The disc center (*green dot*), BMO center (*red dot*), BMO margin (*orange dot line*), and the RNFL defect margin (*yellow dot line*) are marked. (*Right*) Magnified photograph. Two reference lines extend from the fovea to the disc center and BMO center, respectively, (**1**) foveo-disc axis (**a**) and (**2**) foveo-BMO axis (**b**). The minimum angle between the reference line and a line from the center of the disc or BMO to the margin of the RNFL defect (*yellow dot*) close to the fovea (angle $\alpha$), and a line to the margin of the RNFL defect (*yellow dot*) further from the fovea (angle $\beta$), was measured from the two reference lines: (**1**) angle $\alpha_{disc}$ and angle $\beta_{disc}$ and (**2**) angle $\alpha_{BMO}$ and angle $\beta_{BMO}$. Angle $\gamma$ is the angular width of the RNFL defect, as calculated by the difference between angle $\beta_{BMO}$ and angle $\alpha_{BMO}$.

## Measurement of Angular Parameters of RNFL Defect

For the measurement, images of the infrared SD-OCT were superimposed and aligned to red-free fundus photographs according to retinal landmarks, such as central retinal vasculature and central retinal vascular trunk, using a commercially available software (Photoshop; Adobe, San Jose, CA). To complete this process, images were enlarged and placed as needed. The layers of OCT became transparent with opacity set to 50%, so that the underlying images of photographs showed through.

To quantify the angular extent of the RNFL defect, the parameters were defined as follows (Fig. 1).

(1) Reference lines: two reference lines extending from the fovea to the disc center and to the BMO center (foveo-disc axis and foveo-BMO axis, respectively)

(2) Angle $\alpha_{disc}$: the minimum angle between the reference line of the foveo-disc axis and a line from the center of the disc to the margin of the RNFL defect bordering on the BMO close to the fovea

(3) Angle $\alpha_{BMO}$: the minimum angle between the reference line of the foveo-BMO axis and a line from the center of the BMO to the margin of the RNFL defect bordering on the BMO close to the fovea

(4) Angle $\beta$: the minimum angle between the reference line and a line from the center of the disc or BMO to the margin of the RNFL defect further from the fovea (angle $\beta_{disc}$ and angle $\beta_{BMO}$, respectively)

(5) Angle $\gamma$: the angular width of the RNFL defect measured from the BMO center (angle $\beta_{BMO}$–angle $\alpha_{BMO}$)

(6) $\Delta\alpha$: the difference of angle $\alpha$ as measured from the disc and BMO centers (angle $\alpha_{BMO}$–angle $\alpha_{disc}$)

The angles were measured using ImageJ software version 1.51 (National Institutes of Health). All of the measurements were obtained by the two glaucoma specialists (EB, KML) respectively blinded to information on the patients' clinical history. We used the average of the two measurements for each parameter. When there were multiple RNFL defects, the defect closest to the reference line was analyzed for angular location. The total width was calculated by summing all of the defects of the eye.

## Statistical Analyses

The categorical variables were compared with chi-squared tests. The continuous variables were compared with *t*-tests and ANOVA tests that had been corrected for multiple comparisons according to the Bonferroni method. Interobserver reproducibility for disc center determination was evaluated by the pixel values of the x and y coordinates obtained by two independent observers (EB and KML). The standard deviation of difference and coefficient of variation were calculated. Intraobserver reproducibility was assessed based on two measurements by one observer (EB), at intervals of at least 1 week. Pearson correlation coefficient (*r*) and linear regression analysis were used. A univariate logistic regression analysis was performed to evaluate the factors associated with the difference of angle $\alpha$ as measured from the disc and BMO centers, respectively. The variables that retained significance at $P < 0.10$ were included in a subsequent multivariate model. Statistical analyses were performed with the Statistical Package for Social Sciences version 21.0 for Windows (SPSS, Inc., Chicago, IL). A *P* value <0.05 was considered to represent statistical significance.

## RESULTS

A total of 141 eyes of 141 patients with OAG with localized RNFL defect were initially enrolled. Of these, 23 patients were excluded: 5 eyes with posterior staphyloma, 2 eyes diagnosed as steroid-induced glaucoma, 9 eyes with poor quality of RNFL photography, and 7 eyes with low-signal-strength OCT images, including one eye with difficulty in identifying the BMO. The final study patients included 118 patients with 118 eyes. The patients' demographic and baseline ocular characteristics are presented in Tables 1 and 2. By classifying patients according to the degree of myopia, 40 eyes with high myopia, 42 eyes with mild to moder-

TABLE 1. Demographic Data and Angle Parameters of Groups Based on Myopia

| Variable | High Myopia (A) ($n= 40$) | Mild-to-Moderate Myopia (B) ($n= 42$) | Nonmyopia (C) ($n= 36$) | P Value | Post Hoc Analysis |
|---|---|---|---|---|---|
| Demographics | | | | | |
|   Glaucoma subtype | | | | | |
|     NTG | 26 (65.0) | 22 (52.4) | 16 (44.4) | 0.19 | NS |
|     HTG | 14 (35.0) | 20 (47.6) | 20 (55.6) | | |
|   Age, y | $46.2 \pm 13.6$ | $53.4 \pm 10.4$ | $63.6 \pm 10.1$ | **<0.001** | A<B<C |
|   Male | 36 (90.0) | 26 (61.9) | 22 (61.1) | **0.006** | A<B, C |
|   MD, dB | $-6.10 \pm 4.80$ | $-5.59 \pm 4.62$ | $-4.90 \pm 5.48$ | 0.30 | NS |
| Angle Parameters, deg | | | | | |
|   Angle $\alpha$-disc | $30.1 \pm 13.3$ | $39.3 \pm 13.3$ | $43.8 \pm 16.2$ | **0.001** | A<B, C |
|   Angle $\alpha$-BMO | $38.2 \pm 18.8$ | $44.2 \pm 18.6$ | $44.7 \pm 19.3$ | 0.19 | NS |
|   Angle $\alpha$ difference | $8.4 \pm 5.8$ | $6.7 \pm 5.2$ | $3.2 \pm 2.2$ | **<0.001** | A<B, C |
|   Angle $\gamma$ | $50.1 \pm 18.1$ | $47.8 \pm 15.2$ | $44.2 \pm 19.9$ | 0.37 | NS |

    Comparison was performed using one-way ANOVA with post hoc Bonferroni correction for multiple comparisons. Values with statistical significance are shown in bold.

    NTG = normal-tension glaucoma; HTG = high-tension glaucoma; MD = mean deviation; dB = decibel; BMO = Bruch's membrane opening.

TABLE 2. Demographic Data and Angle Parameters of Groups Based on Open-Angle Glaucoma

| Variable | NTG ($n = 64$) | HTG ($n = 54$) | P Value |
|---|---|---|---|
| Demographics | | | |
|   Myopia | | | |
|     High myopia | 26 (40.6) | 14 (25.9) | 0.07 |
|     Mild to moderate myopia | 22 (34.3) | 20 (37.0) | |
|     Nonmyopia | 16 (25.0) | 20 (37.0) | |
|   Age, y | $52.7 \pm 13.4$ | $55.8 \pm 13.4$ | 0.17 |
|   Male | 45 (70.3) | 39 (72.2) | 0.82 |
|   Axial length, mm | $25.55 \pm 1.89$ | $24.99 \pm 1.73$ | 0.70 |
|   MD, dB | $-5.53 \pm 4.26$ | $-5.58 \pm 5.70$ | 0.55 |
| Angle parameters, deg | | | |
|   Angle $\alpha$-disc | $37.2 \pm 16.2$ | $35.4 \pm 17.6$ | 0.52 |
|   Angle $\alpha$-BMO | $44.3 \pm 19.7$ | $37.3 \pm 17.1$ | 0.25 |
|   Angle $\alpha$ difference | $7.2 \pm 3.6$ | $4.1 \pm 2.4$ | **0.023** |
|   Angle $\gamma$ | $47.5 \pm 16.8$ | $48.5 \pm 18.3$ | 0.92 |

    Values are presented as number (%) or mean ± SD. Comparison was performed using an independent *t* test. Values with statistical significance are shown in bold.

### Reproducibility of Determined Optic Disc Center

The reproducibility of the optic disc center was evaluated based on the x and y coordinate values of the pixels obtained by two independent observers (Supplementary Figure S1).[28] The interobserver reliability was excellent (x-axis: standard deviation of difference = 5.339 pixels, y-axis: standard deviation of difference = 6.508 pixels). Coefficient of variation was estimated using the one-way ANOVA random-effects
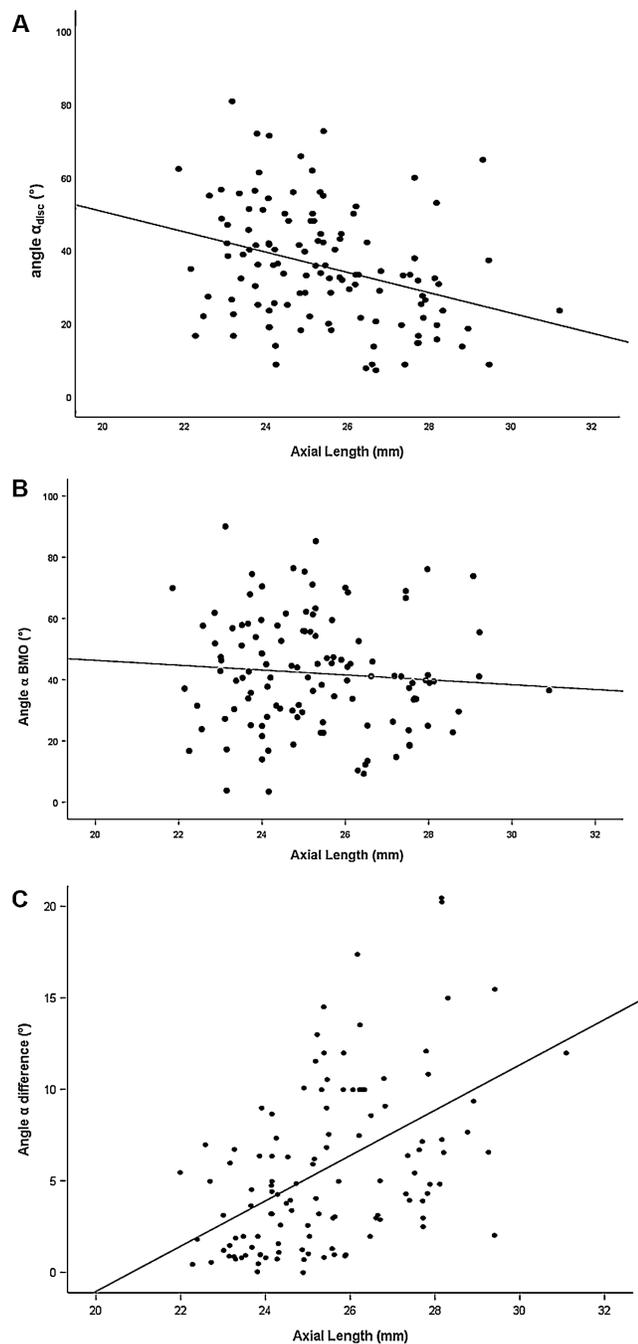
model: 0.370% along the x-axis and 0.345% along the y-axis. The intraobserver reliability was also excellent (x-axis: standard deviation of difference = 3.470 pixels, y-axis: standard deviation of difference = 3.618 pixels). Coefficient of variation was estimated using the one-way ANOVA random-effects model: 0.254% along the x-axis and 0.189% along the y-axis. Supplementary Table S1 provides the inter- and intraobserver reliabilities of the optic disc center and the distance between the disc and BMO centers in subgroups according to the degree of myopia.

### Subgroups Based on Myopia

Angle $\alpha_{disc}$ showed significant differences among the three groups with RNFL defects close to the fovea in highly myopic eyes: 30.1° ± 13.3° in high myopia, 39.3° ± 13.3° in mild to moderate myopia, and 43.8° ± 16.2° in nonmyopia (Table 1, $P = 0.001$). Bonferroni's post hoc analysis revealed that patients with highly myopic eyes had a significantly smaller angle $\alpha_{disc}$ than did those with mild to moderate or nonmyopic eyes. A significant correlation between angle $\alpha_{disc}$ and AL ($r = -0.327$, $P = 0.001$) (Fig. 2A) was identified. However, angle $\alpha_{BMO}$ showed no significant differences among the three myopia groups by ANOVA: 38.2° ± 18.8° in high myopia, 44.2° ± 18.6° in mild to moderate myopia, and 44.7° ± 19.3° in nonmyopia (Table 1, $P = 0.19$). Angle $\alpha_{BMO}$ presented no significant association with AL ($r = -0.080$, $P = 0.39$) (Fig. 2B). The angle $\alpha$ difference ($\Delta\alpha$) was significantly larger in highly myopic eyes than in mild to moderate or nonmyopic eyes by ANOVA with post hoc analysis (Table 1, $P < 0.001$ for all). Mild to moderately myopic eyes showed marginally significantly larger $\Delta\alpha$ relative to nonmyopic eyes ($P = 0.07$). There was a significant correlation between $\Delta\alpha$ and AL ($r = 0.471$, $P < 0.001$) (Fig. 2C). The width of the RNFL defect (angle $\gamma$) showed no differences among the myopic subgroups. Representative cases classified by myopia are presented in Figure 3.
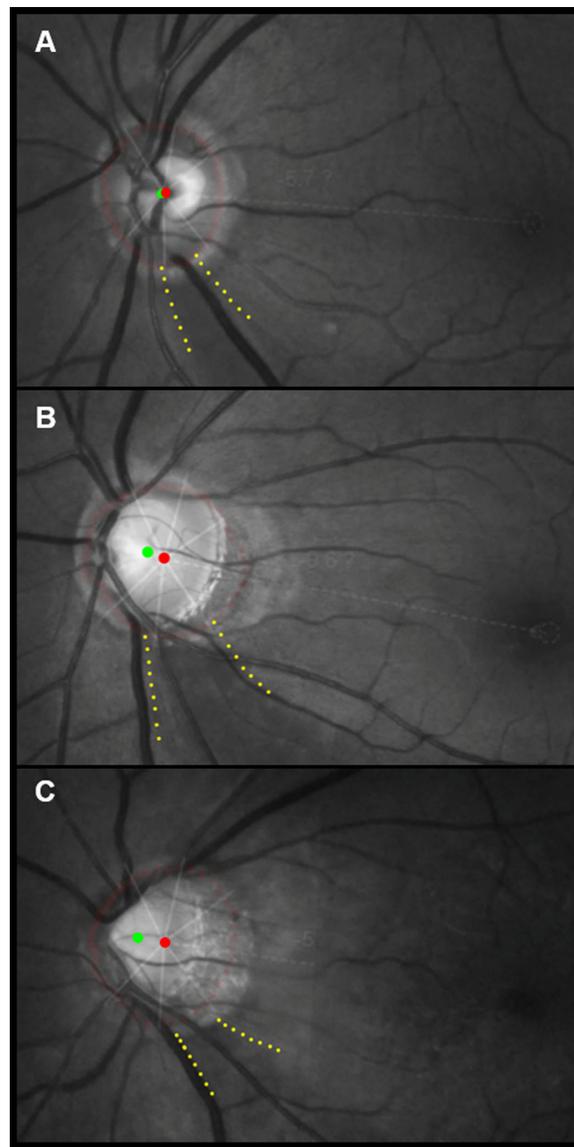
### Subgroups Based on OAG Diagnosis

A comparison of the angle parameters between the two OAG groups is provided in Table 2. The $\Delta\alpha$ was statistically larger in the NTG group than in the HTG group (7.2° ± 3.6° vs. 4.1°

ate myopia, and 36 nonmyopic eyes were reviewed. The average AL was 27.41 ± 1.07 (range, 26.5–30.9) in high myopia, 24.97 ± 0.51 (range, 24.0–25.9) in mild to moderate myopia, and 23.32 ± 0.59 (range, 21.9–23.9) in nonmyopic eye ($P < 0.001$). Patients in the nonmyopia group were significantly older than those in the other, myopia groups ($P < 0.001$). Based on the classification of patients with OAG, there were 64 NTG eyes and 54 HTG eyes. Mean age, sex, AL, and baseline MD showed no significant intergroup differences.

**FIGURE 2.** Scatterplots presenting the association with axial length and angular parameters by linear regression analysis. *Black lines* indicate the best-fit linear regression line. $r$ = correlation coefficient from the fitted linear regression model. (**A**) Angle $\alpha_{disc}$ had significant correlation with axial length ($r = -0.327$, $P = 0.001$). (**B**) No significant correlation was demonstrated between angle $\alpha_{BMO}$ and axial length ($r = -0.080$, $P = 0.39$). (**C**) Angle $\alpha$ difference had significant correlation with axial length ($r = 0.471$, $P < 0.001$). BMO = Bruch's membrane opening.



**FIGURE 3.** Representative cases of RNFL defect compared for disc center and BMO center in eyes with nonmyopia, mild to moderate myopia, and high myopia. RNFL photographs merged with spectral-domain optical coherence tomography images locating the disc center (*green dot*), the BMO margin (*red dotted line*), the BMO center (*red dot*), and the RNFL defect (*yellow dotted line*). Note the position of the disc center relative to the BMO center. (**A**) Left eye of a 62-year-old man with nonmyopia and AL of 23.6 mm. He was diagnosed with HTG, and the baseline MD was −2.25 dB (angle $\alpha_{disc}$: 43.3°, angle $\alpha_{BMO}$: 45.7°, $\Delta\alpha$: 2.3°, angle $\gamma$: 39.4°). (**B**) Left eye of a 46-year-old woman with mild to moderate myopia and AL of 24.99 mm. She had previously been diagnosed with HTG, and the baseline MD was −4.32 dB (angle $\alpha_{disc}$: 39.7°, angle $\alpha_{BMO}$: 45.9°, $\Delta\alpha$: 5.2°, angle $\gamma$: 45.1°). (**C**) Left eye of a 64-year-old man with high myopia and AL of 26.7 mm. He was diagnosed with normal-tension glaucoma, and the baseline MD was −5.54 dB (angle $\alpha_{disc}$: 34.5°, angle $\alpha_{BMO}$: 43.4°, $\Delta\alpha$: 8.9°, angle $\gamma$: 40.5°).

## Factors Associated With Angle $\alpha$ Difference

The factors associated with $\Delta\alpha$ were determined by univariate and multivariate logistic regression analyses (Table 3). By the multivariate analysis, AL and NTG diagnoses were

± 2.4°, $P = 0.023$). None of the other parameters differed with statistical significance.

**TABLE 3.** Factors Associated With Angle $\alpha$ Difference

| Variable | Univariate Analysis | | | Multivariate Analysis[*] | | |
|---|---|---|---|---|---|---|
| | Coefficient | 95% CI | *P* Value | Coefficient | 95% CI | *P* Value |
| Age, y | −0.136 | (−0.203 to −0.072) | <0.001 | −0.069 | (−0.139 to 0.001) | 0.10 |
| Male | 0.840 | (−1.181 to 2.849) | 0.48 | | | |
| Axial length, mm | **1.183** | **(0.758 to 1.644)** | **<0.001** | **0.899** | **(0.323 to 1.343)** | **0.002** |
| Glaucoma subtype | **−2.513** | **(−4.514 to −0.981)** | **0.010** | **−2.053** | **(−3.616 to −0.454)** | **0.021** |

[*]Adjusted for all variables with P < 0.1 in a univariable regression model. Values with statistical significance are shown in bold.

significantly associated with $\Delta\alpha$ (*P* = 0.002, 0.021, respectively).

## DISCUSSION

In the present study, we investigated the angular location of the RNFL defect in OAG as related to myopia and glaucoma subtypes. The RNFL defect was closer to the fovea when measured from the disc as opposed to the BMO center in myopic eyes, while the angular location of the RNFL defect did not differ between the OAG subtypes.

Previous studies on highly myopic eyes in OAG have reported the location of the RNFL defect to be close to the fovea.[7–9] It has been posited that mechanical stress on the sclera during axial elongation may generate tensile stretch on the temporal edge of the LC and RGC axons, leading to RFNL defects close to the fovea.[9,29,30] However, none of the relevant reports could clearly explain the mechanism of RNFL defects' locational pattern associated with myopia. In the present study, we were able to suggest the mechanism of the locational pattern of the RNFL defect in myopic glaucomatous eyes. Recently, in the Boramae Myopia Cohort Study, we found that the inner retinal structure of the posterior polar area, including the BMO, was relatively preserved during axial elongation, while the outer loadbearing structure expanded.[19–21] This expansion of the sclera and consequent shift of the LC from the preserved BMO results in the change of ONH shape that is seen in myopia: border-tissue rotation from the internally oblique to the externally oblique direction and expansion of the temporal externally oblique border and sclera. In line with Sawada et al.[18] that in most myopic eyes, the clinical disc margin was the BMO in the nasal half and the anterior scleral opening in the temporal half of the optic disc, these ONH changes during axial elongation induced a nasal shift of the ONH center from the relatively preserved BMO center. As the posterior polar retinal structures including RNFL bundle trajectories remained relatively stable during axial elongation[19–21] and as the RNFL defect began in the vulnerable area of the LC (Fig. 4), we assumed that the RNFL defect presents locational difference relative to (1) the disc center, which changes nasally, or (2) the BMO center, which is a relatively stable structure. In our study, the angular location of the RNFL defect measured from the disc center was smaller than when measured from the BMO for eyes with longer AL. Therefore, we may deduce that funduscopically visualized optic disc margin change associated with axial elongation might influence the characteristic features of the RNFL defect in myopic glaucomatous eyes.

On the other hand, the angular location of the RNFL defect as measured from the BMO center was independent of AL. Also, the angular difference as measured from the disc and BMO centers was notably significant in highly myopic eyes. Although mild to moderate myopia also had a greater angular difference compared with nonmyopia, it did not attain statistical significance. This can be explicated by the relatively small disc displacement from the BMO center in mild to moderate myopia eyes as compared with the wide extent of disc displacement in highly myopic eyes (Fig. 3).

To date, the angular location of the RNFL defect in OAG subtypes has been investigated but seems uncertain with discordant data. Previous reports presenting no difference in the spatial pattern of RNFL defects between NTG and HTG suggested that they undergo the same pathologic process.[13–16] Conversely, other studies have reported positive differences with the RNFL defect closer to the fovea in NTG.[11,12] They suggested that there may be more than one pathogenic mechanism in the development of RNFL defects in NTG and explained these findings in relation to enlargement of the optic disc in the papillomacular bundle area or distortion of the LC, which is prominent in NTG. Unfortunately, one of the above-noted studies did not evaluate the patients' myopic degree.[11] In our study, the angular location of the RNFL defect did not differ between NTG and HTG, both measured from the disc and BMO center. However, remarkably, the difference in angle measured from the center of the disc and BMO was greater in NTG than in HTG. An angle $\alpha$ difference stands for the offset between the BMO and optic disc margin. A possible explanation is that NTG eyes were exposed to a larger offset during the same amount of axial elongation, which makes it more vulnerable to the IOP-associated damage. Additionally, in our previous report on myopic NTG, there was a large extent of LC shift associated with AL.[22] However, other selection biases may have occurred, and a larger population-based study would be necessary to elucidate this issue.

The width of the RNFL defect is associated with visual field sensitivity abnormality.[31] In our study, no marked difference in baseline MD values or width of the RNFL defect among the subgroups of myopia and glaucoma was apparent. Also, Kimura et al.[9] reported no difference in width of the RNFL defect between high myopia and nonhigh myopia after adjusting the MD value. By contrast, however, Kim et al.[7] reported that highly myopic patients with OAG presented wider RNFL defects compared with non–highly myopic patients. The authors, however, enrolled highly myopic patients with significantly reduced MD values relative to the low to moderate myopia and emmetropia groups. The different baseline values of MD might have led to a conclusion that highly myopic eyes have wider defects.

The present study has some limitations. First, it was performed according to a cross-sectional design, and so, assessment of the changes of the measured parameters was impossible. Second, the sample size was relatively small in a single hospital, and all patients were Korean. A potential selection bias might have influenced the results
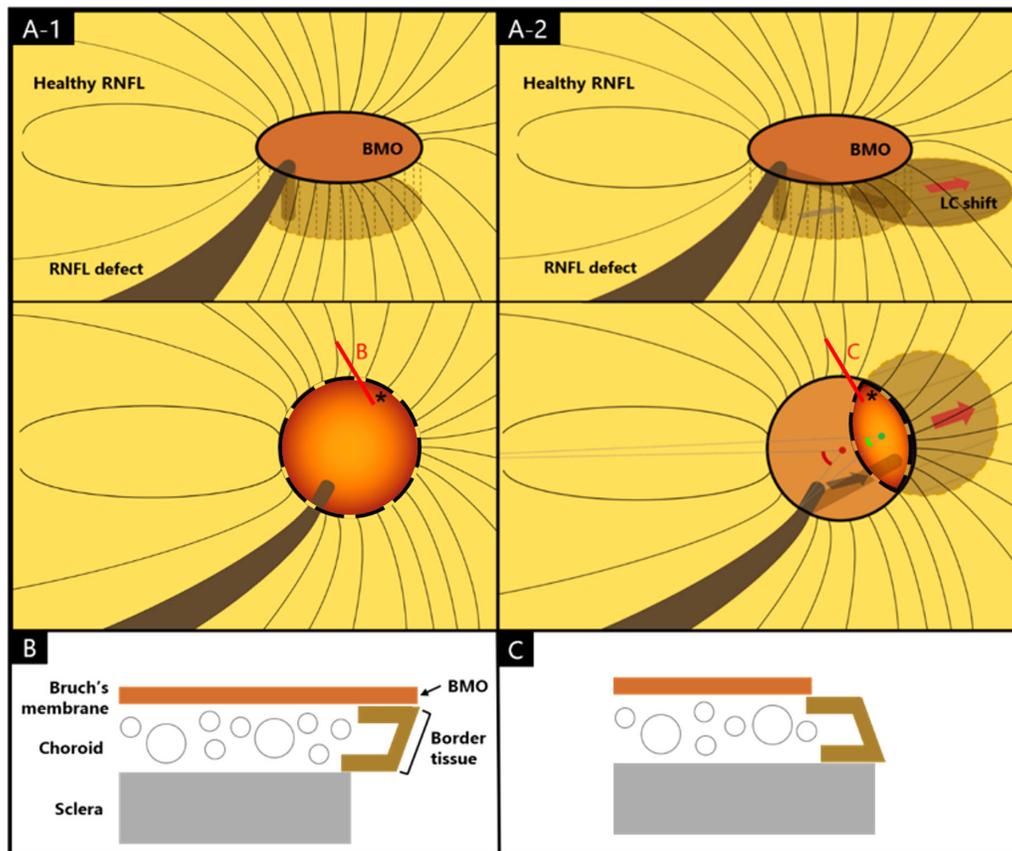
**FIGURE 4.** Schematic summary of the anatomic change with lamina cribrosa shift (LC): (**A-1**) Before LC shift. (*Top row*) High viewpoint tilted diagonally. (*Middle row*) High viewpoint straight down. The overlying layer consists of a healthy RNFL (*bright yellow*), RNFL defect (*dark brown*), and the BMO (*orange plane*). The underlying layer consists of the LC (*light-brown plane*). *The funduscopically visible disc margin is marked by a *dotted line*, which does not always consistent with the BMO. (**A-2**) After LC shift in myopia. (*Top row*) High viewpoint tilted diagonally. (*Middle row*) High viewpoint straight down. During axial elongation, the underlying initial LC (*light-brown plane*) shifts in the *red-arrow* direction (*hatched light-brown plane*), which induces a shift (*gray arrow*) of the vulnerable LC area. Contrastingly, the location of RNFL bundle trajectories relative to the BMO remains relatively stable. The optic disc is indicated as the *oval bright orange plane* with a *dotted line*. *The optic disc margin is marked by a *dotted line*, as it does not correspond to a unique anatomical structure but to a complex interaction of structures.[18,33] *Reference lines* extending from the fovea (*transversal gray dotted lines*) to the disc center (*green dot*) and BMO center (*red dot*) are lined up with the margin of the RNFL defect close to the fovea, respectively. Note the angular location of the RNFL defect (angle $\alpha$) compared from the disc and BMO center; angle $\alpha_{disc}$ (*green angle*) versus angle $\alpha_{BMO}$ (*red angle*). As the LC shifts during axial elongation, the angle $\alpha_{disc}$ gets smaller, compared to the stable angle $\alpha_{BMO}$. The *red line* passes over the clinically identified optic disc margin (*black dotted line*). (**B**, **C**) Schematic representation of changes occurring on border tissue configuration during LC shift. (**B**) Border tissue structure before LC shift: internally oblique relative to the underlying sclera. (**C**) Border tissue structure after LC shift: externally oblique relative to the underlying sclera. Modified from the figure previously published in Reis ASC, Sharpe GP, Yang H, et al. Optic disc margin anatomy in patients with glaucoma and normal controls with spectral domain optical coherence tomography. *Ophthalmology*. 2012;119:738–747.

and rendered the present findings ungeneralizable to other ethnic groups. Further, follow-up studies with large sample sizes representative of other ethnic groups are required. Third, the margin of the RNFL defect was traced from the boundary of the BMO for all angle $\alpha$ measurements. Tracing the margin from the boundary of the optic disc is not possible in patients with large peripapillary atrophy (Fig. 3). Extending the margin of the RNFL defect bordering on the BMO boundary toward the disc boundary could have incurred inaccuracies, leading to measurement error. Fourth, when identifying the disc margin anatomy, the complexity of the disc margin and subjectivity of its location according to the examiner should be considered. The disc margin does not correspond to a unique anatomical structure but to a complex interaction of structures (i.e., border tissue, anterior scleral opening, and BMO).[18,32] Different exam-

iners may have different impressions on the disc margin location, which may produce somewhat different results. However, the center of optic disc, obtained by two independent observers, showed excellent reliability. We speculated that the center of the optic disc would be affected to a lesser degree than the exact margin of it. Fifth, the present study focused on the structural location of the RNFL defect as associated with myopia, while the pattern of VF defect was not evaluated. Previous studies have reported on high myopia as associated with a distinct pattern of VF defect.[9] Further studies exploring the patterns of VF defect associated with myopia will be necessary in order to elucidate that association.

In conclusion, we compared the angular location of the RNFL defect in myopic OAG, acquired from the disc and BMO center. The RNFL defect measured from the disc center,

as associated with longer AL, was closer to the fovea, while no association was found from the BMO center. There was no locational difference between OAG subtypes. These findings may facilitate understanding of the characteristic locational pattern of the RNFL defect in myopic glaucomatous eyes.

## References

1. Weinreb RN, Aung T, Medeiros FA. The pathophysiology and treatment of glaucoma: a review. *JAMA*. 2014;311:1901–1911.

2. Quigley HA, Addicks EM. Regional differences in the structure of the lamina cribrosa and their relation to glaucomatous optic nerve damage. *Arch Ophthalmol*. 1981;99:137–143.

3. Abe RY, Gracitelli CPB, Diniz-Filho A, Tatham AJ, Medeiros FA. Lamina cribrosa in glaucoma: diagnosis and monitoring. *Curr Ophthalmol Rep*. 2015;3:74–84.

4. Tatham AJ, Miki A, Weinreb RN, Zangwill LM, Medeiros FA. Defects of the lamina cribrosa in eyes with localized retinal nerve fiber layer loss. *Ophthalmology*. 2014;121:110–118.

5. Kanamori A, Nakamura M, Tomioka M, Kawaka Y, Yamada Y, Negi A. Structure-function relationship among three types of spectral-domain optical coherent tomography instruments in measuring parapapillary retinal nerve fibre layer thickness. *Acta Ophthalmol*. 2013;91:e196–202.

6. Kanamori A, Nakamura M, Escano MF, Seya R, Maeda H, Negi A. Evaluation of the glaucomatous damage on retinal nerve fiber layer thickness measured by optical coherence tomography. *Am J Ophthalmol*. 2003;135:513–520.

7. Kim JM, Park KH, Kim SJ, et al. Comparison of localized retinal nerve fiber layer defects in highly myopic, myopic, and non-myopic patients with normal-tension glaucoma: a retrospective cross-sectional study. *BMC Ophthalmology*. 2013;13:67.

8. Chihara E, Sawada A. Atypical nerve fiber layer defects in high myopes with high-tension glaucoma. *Arch Ophthalmol*. 1990;108:228–232.

9. Kimura Y, Hangai M, Morooka S, et al. Retinal nerve fiber layer defects in highly myopic eyes with early glaucoma. *Invest Ophthalmol Vis Sci*. 2012;53:6472–6478.

10. Greve EL, Furuno F. Myopia and glaucoma. *Albrecht von Graefes Arch Klin Exp Ophthalmol*. 1980;213:33–41.

11. Woo SJ, Park KH, Kim DM. Comparison of localised nerve fibre layer defects in normal tension glaucoma and primary open angle glaucoma. *Br J Ophthalmol*. 2003;87:695–698.

12. Chihara E, Tanihara H. Parameters associated with papillomacular bundle defects in glaucoma. *Graefes Arch Clin Exp Ophthalmol*. 1992;230:511–517.

13. Mok KH, Lee VW, So KF. Retinal nerve fiber loss pattern in high-tension glaucoma by optical coherence tomography. *J Glaucoma*. 2003;12:255–259.

14. Mok KH, Lee VW, So KF. Retinal nerve fiber loss in high- and normal-tension glaucoma by optical coherence tomography. *Optom Vis Sci*. 2004;81:369–372.

15. Konstantakopoulou E, Reeves BC, Fenerty C, Harper RA. Retinal nerve fiber layer measures in high- and normal-tension glaucoma. *Optom Vis Sci*. 2008;85:538–542.

16. Baniasadi N, Paschalis EI, Haghzadeh M, et al. Patterns of retinal nerve fiber layer loss in different subtypes of open angle glaucoma using spectral domain optical coherence tomography. *J Glaucoma*. 2016;25:865–872.

17. Chauhan BC, Danthurebandara VM, Sharpe GP, et al. Bruch's membrane opening minimum rim width and retinal nerve fiber layer thickness in a normal white population: a multicenter study. *Ophthalmology*. 2015;122:1786–1794.

18. Sawada Y, Araie M, Shibata H, Ishikawa M, Iwata T, Yoshitomi T. Optic disc margin anatomic features in myopic eyes with glaucoma with spectral-domain OCT. *Ophthalmology*. 2018;125:1886–1897.

19. Kim M, Choung HK, Lee KM, Oh S, Kim SH. Longitudinal changes of optic nerve head and peripapillary structure during childhood myopia progression on OCT: Boramae Myopia Cohort Study Report 1. *Ophthalmology*. 2018;125:1215–1223.

20. Lee KM, Choung HK, Kim M, Oh S, Kim SH. Positional change of optic nerve head vasculature during axial elongation as evidence of lamina cribrosa shifting: Boramae Myopia Cohort Study Report 2. *Ophthalmology*. 2018;125:1224–1233.

21. Lee KM, Choung HK, Kim M, Oh S, Kim SH. Change of betazone parapapillary atrophy during axial elongation: Boramae Myopia Cohort Study Report 3. *Invest Ophthalmol Vis Sci*. 2018;59:4020–4030.

22. Lee KM, Kim M, Oh S, Kim SH. Position of central retinal vascular trunk and preferential location of glaucomatous damage in myopic normal-tension glaucoma. *Ophthalmol Glaucoma*. 2018;1:32–43.

23. Hoyt WF, Frisén L, Newman NM. Fundoscopy of nerve fiber layer defects in glaucoma. *Invest Ophthalmol Vis Sci*. 1973;12:814–829.

24. Nitta K, Sugiyama K, Wajima R, Tachibana G. Is high myopia a risk factor for visual field progression or disk hemorrhage in primary open-angle glaucoma? *Clin Ophthalmol*. 2017;11:599–604.

25. Ohsugi H, Ikuno Y, Shoujou T, Oshima K, Ohsugi E, Tabuchi H. Axial length changes in highly myopic eyes and influence of myopic macular complications in Japanese adults. *PloS One*. 2017;12:e0180851.

26. Almazroa A, Alodhayb S, Osman E, et al. Agreement among ophthalmologists in marking the optic disc and optic cup in fundus images. *Int Ophthalmol*. 2017;37:701–717.

27. Aptel F, Denis P. Optical coherence tomography quantitative analysis of iris volume changes after pharmacologic mydriasis. *Ophthalmology*. 2010;117:3–10.

28. Rosner B. *Fundamentals of Biostatistics*. 8th ed. Boston, MA: Rita Lombard; 2016:605–609.

29. Kim TW, Kim M, Weinreb RN, Woo SJ, Park KH, Hwang JM. Optic disc change with incipient myopia of childhood. *Ophthalmology*. 2012;119:21–26.e21–23.

30. Ohno-Matsui K, Akiba M, Moriyama M, et al. Acquired optic nerve and peripapillary pits in pathologic myopia. *Ophthalmology*. 2012;119:1685–1692.

31. Lee MJ, Kim DM, Jeoung JW, Hwang SS, Kim TW, Park KH. Localized retinal nerve fiber layer defects and visual field abnormalities by Humphrey matrix frequency doubling technology perimetry. *Am J Ophthalmol*. 2007;143:1056–1058.

32. Hong SW, Koenigsman H, Ren R, et al. Glaucoma specialist optic disc margin, rim margin, and rim width discordance in glaucoma and glaucoma suspect eyes. *Am J Ophthalmol*. 2018;192:65–76.

33. Reis AS, Sharpe GP, Yang H, Nicolela MT, Burgoyne CF, Chauhan BC. Optic disc margin anatomy in patients with glaucoma and normal controls with spectral domain optical coherence tomography. *Ophthalmology*. 2012;119:738–747.